LETTERS
https://doi.org/10.1038/s41567-022-01671-3

nature physics

Chiral cavity quantum electrodynamics

John Clai Owens[1,2], Margaret G. Panetta[1], Brendan Saxberg[1], Gabrielle Roberts[1], Srivatsan Chakram[3], Ruichao Ma[4], Andrei Vrajitoarea[1], Jonathan Simon[1] and David I. Schuster[1]✉

Cavity quantum electrodynamics, which explores the granularity of light by coupling a resonator to a nonlinear emitter[1], has played a foundational role in the development of modern quantum information science and technology. In parallel, the field of condensed matter physics has been revolutionized by the discovery of underlying topological[2–4], often arising from the breaking of time-reversal symmetry, as in the case of the quantum Hall effect. In this work, we explore the cavity quantum electrodynamics of a transmon qubit in a topologically nontrivial Harper–Hofstadter lattice[5]. We assemble the lattice of niobium superconducting resonators[6] and break time-reversal symmetry by introducing ferrimagnets[7] before coupling the system to a transmon qubit. We spectroscopically resolve the individual bulk and edge modes of the lattice, detect Rabi oscillations between the excited transmon and each mode and measure the synthetic-vacuum-induced Lamb shift of the transmon. Finally, we demonstrate the ability to employ the transmon to count individual photons[8] within each mode of the topological band structure. This work opens the field of experimental chiral quantum optics[9], enabling topological many-body physics with microwave photons [10,11] and providing a route to backscatter-resilient quantum communication.

Materials made of light are a frontier in quantum many-body physics[12]. Relying upon nonlinear emitters to generate strong photon–photon interactions and ultra-low-loss meta-materials to manipulate the properties of the individual photons, this field explores the interface of condensed matter physics and quantum optics while simultaneously producing devices for manipulating light[13,14]. Recent progress in imbuing photons with topological properties[15], wherein the photons undergo circular time-reversal-breaking orbits, promises opportunities to explore photonic analogues of such solid-state phenomena as the (fractional) quantum Hall effect[2,3], Abrikosov lattices[16] and topological insulators[4].

In electronic materials, the circular electron orbits result from magnetic or spin–orbit couplings[4]. Unlike electrons, photons are charge-neutral objects and so do not couple directly to magnetic fields. There is thus an effort to generate synthetic magnetic fields for photons and more generally to explore ideas of topological quantum matter in synthetic photonic platforms. Significant progress in this arena has been made in both optical and microwave topological photonics. In silicon photonics[17,18] and optics[19,20], synthetic gauge fields have been achieved while maintaining time-reversal symmetry by encoding a pseudo-spin in either the polarization or spatial mode. In radiofrequency and microwave meta-materials, models both with time-reversal symmetry[21,22] and with broken time-reversal symmetry have been explored, with the time-reversal symmetry breaking induced either by coupling the light to ferrimagnets in magnetic fields[7,23] or by Floquet engineering[24].

To mediate interactions between photons, a nonlinear emitter or ensemble of nonlinear emitters must be introduced into the system[25]. This has been realized for optical photons by coupling them to Rydberg-dressed atoms, providing the first assembly of two-photon Laughlin states of light[26]. In quantum circuits, a three-site lattice of parametrically coupled transmon qubits enabled observation of chiral orbits of photons/holes[24], and a 1×8 lattice of transmons enabled exploration of Mott physics[27]. In nanophotonics, a topological interface enabled coupling of quantum dots to a topological channel[28] and a resonator realized by closing such a channel on itself[29].

In this work, we demonstrate a scalable architecture for probing interacting topological physics with light. Building on prior room-temperature work[7], we demonstrate a 5×5 array of superconducting resonators that acts as a quarter-flux ($\alpha=1/4$) Hofstadter lattice[5], exhibiting topological bulk and edge modes for the photons that reside within it. We couple a single transmon qubit to the edge of this system, and explore the regime of strong-coupling cavity quantum electrodynamics (QED) for a highly nonlinear emitter interacting with the spectrally resolved modes of a topological band structure.

In Section 2, we introduce our superconducting topological lattice architecture compatible with transmon qubits. We then characterize its properties both spectroscopically and spatially in Section 3. In Section 4, we couple a single transmon qubit to the lattice, employing it to detect and manipulate individual photons in bulk and edge modes of the lattice and to measure the Lamb shift of this synthetic vacuum. In Section 5, we conclude, exploring the opportunities opened by this platform.

A superconducting Hofstadter lattice for microwave photons

In vacuum, photons are neither (1) massive nor (2) charged or (3) confined to two dimensions, the crucial ingredients for quantum Hall physics[2]. To realize these essentials, we follow the road-map laid out in ref. [10]. Microwave photons are trapped in a two-dimensional (2D) array of microwave resonators and thereby confined to two transverse dimensions and imbued with an effective mass due to the finite tunnelling rate between the resonators. Rather than attempting to actually imbue photons with electric charge, we note that, when electrons are confined to a lattice, the entire impact of a magnetic field on their dynamics is encompassed by the Aharonov–Bohm-like phase that they acquire when tunnelling around closed trajectories. We engineer this 'Peierls phase' via the spatial structure of the on-site lattice orbitals.

Figure 1a shows the square Hofstadter lattice that we have developed for this work. Each square in the diagram is a lattice site, implemented as a resonator of frequency $\omega_0\approx2\pi\times9$ GHz, tunnel-coupled

[1]James Franck Institute and Department of Physics, University of Chicago, Chicago, IL, USA. [2]Thomas J. Watson, Sr., Laboratory of Applied Physics and Kavli Nanoscience Institute, California Institute of Technology, Pasadena, CA, USA. [3]Department of Physics and Astronomy, Rutgers University, Piscataway, NJ, USA. [4]Department of Physics and Astronomy, Purdue University, West Lafayette, IN, USA. ✉e-mail: dis@uchicago.edu

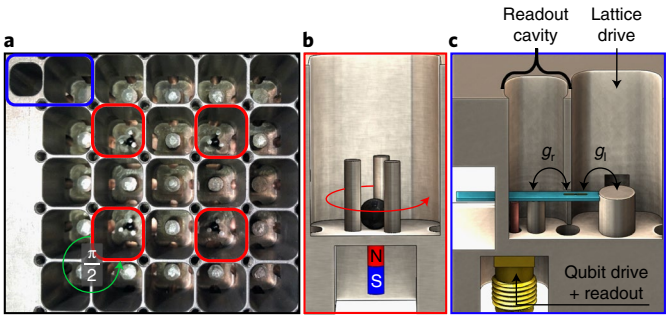

Fig. 1 | Elements of chiral cavity QED. a, The apparatus, consisting of a 5×5, $\alpha = 1/4$ Hofstadter lattice[5] of resonators in which microwave photons propagate as charged particles in a magnetic field, coupled to a single qubit on the edge that is sensitive to the precise number of photons and their energies. Each site, implemented as a coaxial resonator milled into a block of niobium[6], exhibits a resonance frequency ω_0 determined by the length of a central post and a nearest-neighbour tunnelling rate J determined by the size of a machined coupling hole. The synthetic magnetic field manifests as an Aharonov–Bohm flux $\pi/2$ when photons hop around minimal closed loops (green), generated by the spatial structure of the resonator modes: each two-site by two-site plaquette includes one lattice site (red) that exhibits a $p_x + ip_y$ orbital, while the other three sites exhibit s orbitals[7,10]. The additional site (blue) on the system edge serves as readout cavity into which transmons may be inserted. **b**, $p_x + ip_y$ sites instead contain three posts and thus support three microwave modes (s, $p_x \pm ip_y$). Because our Hofstadter lattice employs only the $p_x + ip_y$ mode, we must isolate it. The s mode is tuned away by the electromagnetic coupling between posts, while a YIG ferrimagnet (black) couples primarily to the $p_x - ip_y$ mode (due to the orientation of the B field of the red/blue bar magnet), thereby detuning it in energy and isolating the $p_x + ip_y$ mode. **c**, A transmon qubit is inserted into a gap between readout (left) and lattice (right) cavities on a sapphire carrier (turquoise), and couples to the two cavities with Rabi frequencies g_r and g_l, respectively. A SubMiniature version A (SMA) connector (gold) allows direct microwave probing of this readout cavity and thus the transmon.

to its nearest neighbours with $J = 2\pi \times 18$ MHz (Supplementary Information C). Sites with counter-clockwise red arrows exhibit modes with spatial structure $p_x + ip_y$, while all other sites have s-like modes. The phase winding at a $p_x + ip_y$ site causes photons tunnelling in/out from different directions to acquire a phase ϕ equal to the clockwise angle between the input and output directions[7]. This ensures that, when photons tunnel around a closed loop in the lattice enclosing n plaquettes, they pick up an Aharonov–Bohm-like phase $\phi_{\text{loop}} = n\frac{\pi}{2}$. Such a tight-binding model with a flux per plaquette of $\pi/2$ is called a quarter-flux Hofstadter lattice[5].

To increase the lifetime of photons compared with our prior work[7], we machine the lattice from niobium and cool it to 30 mK, well below the superconducting transition of Nb (see Supplementary Fig. S6 and Methods for details).

Probing the topological lattice

We first characterize the mode structure of the topological lattice itself in the linear regime, before introducing the transmon nonlinearity. Figure 2a shows the anticipated energy spectrum of a semi-infinite strip, $\alpha = 1/4$ Hofstadter lattice with four bands and topologically protected edge channels living below the top band and above the bottom band. In a finite system, these continuum bands and edge channels fragment into individual modes satisfying the boundary conditions. Figure 2b shows the measured response of the lattice when probed spatially both within the bulk (left) and on the edge (right), with the energies aligned to Fig. 2a. It is clear that the bulk spectrum exhibits modes within the bands, while the edge spectrum exhibits modes within the bandgaps. We further validate that the modes we identify as 'bulk' and 'edge' modes reside in the correct spatial location by exciting modes identified with arrows in Fig. 2b and performing microscopy of their spatial structure in Fig. 2c.

To demonstrate that the excitations of the edge channels are indeed both long-lived and travel in a chiral (handed) manner, we excite the system at an edge site with a short pulse (Supplementary Fig. S7) that populates the modes within each of the two bulk energy gaps in Fig. 2d (Supplementary Information F). By monitoring the edge-averaged response, we determine that the high quality factor (Q) of the superconducting cavities enables the excitation to travel the full lattice perimeter >20 times before decay (Fig. 2d). The backscatter-free, unidirectional propagation demonstrates the protection afforded to chiral edge channels by this system's topology. In Fig. 2d (insets), we probe in both space and time and observe that the excitations move in opposite directions in the upper and lower bandgaps, as anticipated from the bulk–boundary correspondence[8]. The difference in group velocities between upper and lower edge channels arises from second-order tunnelling mediated by virtual occupation of the detuned $p_x - ip_y$ cavity modes, where p_x and p_y are first excited resonances of the microwave cavity with nodes along x and y axes, respectively (Supplementary Information F).

Having demonstrated that the topological lattice hosts distinct 'bulk' and 'edge' modes and can support spectrally distinct and long-lived chiral excitations, we couple a nonlinear emitter to the lattice edge, connecting the chirality of this topological band structure with nonlinear effects seen in cavity QED.

Coupling a quantum emitter to the topological lattice

To explore quantum nonlinear dynamics in the topological lattice, we couple it to a transmon qubit (Fig. 1c and Supplementary Information G), which acts as a quantized nonlinear emitter whose properties change with each photon that it absorbs. Unlike traditional cavity and circuit QED experiments in which a nonlinear emitter couples to a single mode of an isolated resonator, here the transmon couples to all modes of the topological lattice. In what follows, we induce a controlled resonant interaction between the transmon and individual lattice modes, investigating the resulting strong-coupling physics.

The $|g\rangle \leftrightarrow |e\rangle$ transition of the transmon ($\omega_q \approx 2\pi \times 7.8$ GHz) is detuned from the lattice spectrum ($\omega_{\text{lattice}} \approx 2\pi \times 9$ GHz) by $\Delta \approx 2\pi \times 1.2$ GHz. We bring the transmon controllably into resonance with individual lattice modes via the dressing scheme in Fig. 3a (inset) (see Methods and ref. [2] for details). This dressing also gives us complete control over the magnitude of the qubit–lattice site coupling.

In Fig. 3a, we tune the excited transmon into resonance with individual lattice modes and observe vacuum-stimulated Rabi oscillations (Supplementary Information I) of a quantized excitation between the transmon and the mode. Comparing with the predicted band structure shown beneath Fig. 3a, we see that the transmon couples efficiently to both bulk and edge modes of the lattice, despite being physically located on the edge. This is because the lattice is only five sites across, comparable to the magnetic length $l_B \approx 1/\alpha = 4$ sites, so the lattice site coupled to the transmon has substantial participation in both bulk and edge modes. Furthermore, the system is sufficiently small that the number of bulk sites is comparable to the number of edge sites, so all modes have approximately the same 'volume'. The rates of Rabi oscillation shown in Fig. 3a reflect the participation of the qubit site in each mode.

To unequivocally demonstrate strong coupling between the transmon and a single lattice mode, we examine a single-frequency slice of Fig. 3a versus evolution time. Figure 3b shows such a slice and demonstrates high-contrast oscillations that take several Rabi

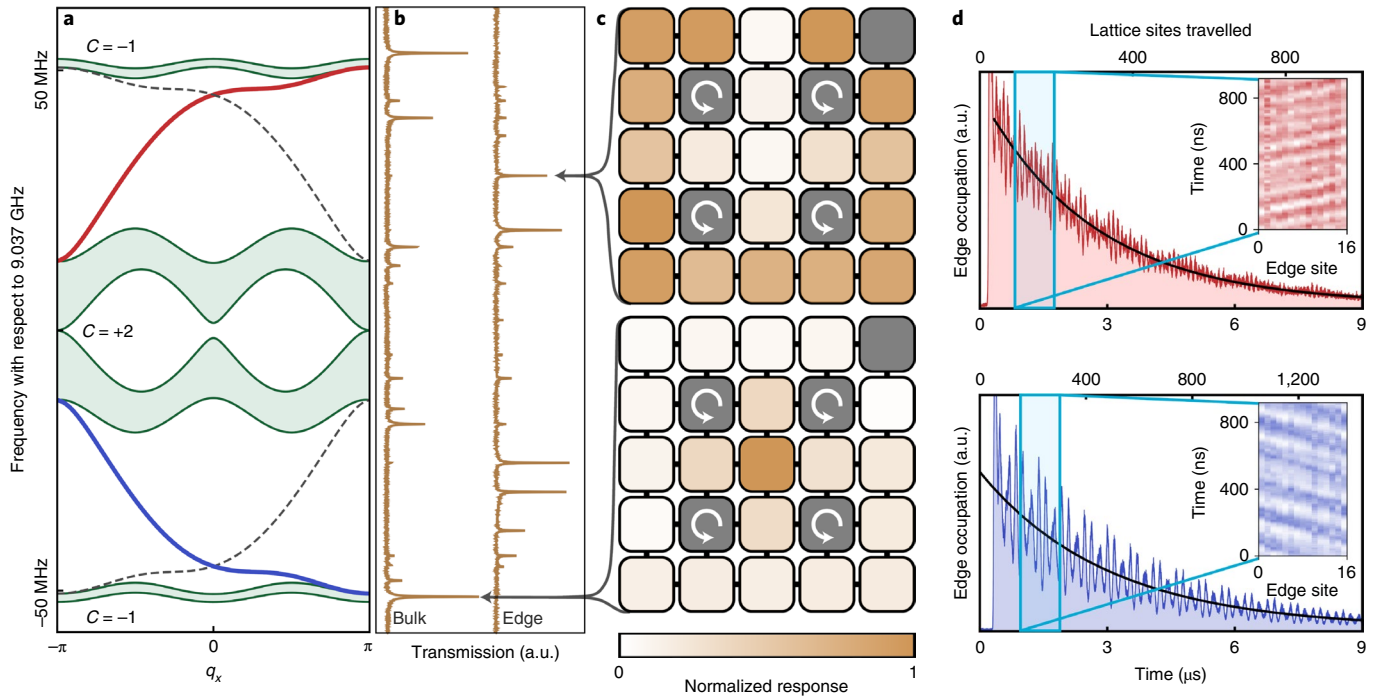

Fig. 2 | A superconducting Chern circuit. The central ingredient of a chiral cavity QED platform is a long-lived, spectrally isolated chiral (unidirectional) mode to couple to a real/synthetic atom. For our experiments, this mode lives on the edge of a synthetic Hall system realized in an $\alpha = 1/4$, Hofstadter square lattice[5]. **a**, The numerically computed band structure of this model (as implemented), for an infinite strip geometry. The top/bottom bands exhibit a Chern number $C = -1$, while the middle two bands, which touch at Dirac points, have a total Chern number of $C = +2$. Chiral edge channels exist above and below the bottom and top bands, respectively, as anticipated from the bulk–boundary correspondence[4]. **b**, Microwave transmission spectra measured through our actual 5 × 5 lattice, where both the bulk bands and chiral edges manifest as well-resolved modes due to the finite system size. 'Bulk' measurements are performed by exciting/measuring at two distinct sites on the lattice interior, while 'Edge' measurements employ two sites on the lattice perimeter. **c**, Measurements of the spatial structure of the modes identified with arrows in **b**, indicating that the mode residing predominantly in the interior of the lattice is located energetically within band, while the one localized to the edge resides within a gap (see Supplementary Information F for measurement details). The 'Normalized response' represents the reflected power normalized to the largest measured power at the chosen drive frequency. Grey squares indicate lattice sites on which these measurements were not performed; those with curved arrows overlaid represent sites hosting ferrite spheres and $p_x + ip_y$ orbitals, while those at the lattice corner identify the site excited in **d**. **d**, The response of the resulting travelling excitation as a function of time averaged over the full perimeter, and versus the site index around the system edge (insets), when a single edge site is excited with a short pulse spectrally centred in the upper/lower (red/blue) gaps. The excitations in the top/bottom bandgaps are centred at 9.064/9.004 GHz. Each Gaussian pulse has a 4σ length of 80 ns. Insets show that upper and lower edge channels have opposite chiralities. The ability of a photon to undergo numerous round trips before decay is equivalent to spectroscopic resolution of the individual edge modes.

cycles to damp out, as is required for strong light–matter coupling. For simplicity, we choose our dressed coupling strength to be less than the lattice mode spacing. Stronger dressing to explore simultaneous coupling to multiple lattice modes opens the realm of super-strong-coupling physics[30,31], where the qubit launches wavepackets localized to smaller than the system size.

When a qubit is tuned towards resonance with a single cavity mode, it experiences level repulsion[32] and then an avoided crossing at degeneracy. The situation is more complex for a qubit coupled to a full lattice, where one must account for interactions with all lattice modes, both resonant and non-resonant. In total, these couplings produce the resonant oscillations observed in Fig. 3b plus a frequency-dependent shift due to level repulsion from off-resonant lattice modes, which may be understood as a Lamb shift from coupling to the structured vacuum[33]. We quantify this Lamb shift by comparing the frequencies of the modes observed in linear lattice spectroscopy, as in Fig. 2b but with the transmon present (Supplementary Information H), with those observed in chevron spectroscopy in Fig. 3a. These data are shown in Fig. 3a (lower inset). When the qubit is tuned near the low-frequency edge of the lattice spectrum, it experiences a downwards shift from all of the modes above it, and when it is tuned near the upper edge of the lattice, it experiences a corresponding upwards shift. These two extremes interpolate smoothly into one another as modes move from one side of the qubit to the other. This effect arises from the multi-modedness of our qubit–cavity system, and not the topology explicitly, as the qubit is coupled only to a single site. There is also a near-constant Stark shift of ~3.5 MHz arising from the classical dressing tone. To our knowledge, this is the first measurement of the Lamb shift of a qubit in a synthetic lattice vacuum.

Finally, we demonstrate the ability to count photons within an individual lattice mode. If the transmon were coupled to a single lattice site and not to the full lattice, each photon in that site would shift the qubit $|g\rangle \leftrightarrow |e\rangle$ transition by 2χ, where $\chi \approx \frac{g_1^2}{\Delta} \times \frac{\alpha_q}{\Delta+\alpha_q} \approx 2\pi \times 5\,\mathrm{MHz}$, and α_q is the transmon anharmonicity. This photon-number-dependent shift, and thus the intra-cavity photon number, can be measured by performing qubit spectroscopy detected through the readout cavity (Supplementary Information K). When the transmon is coupled to a lattice rather than an isolated cavity, the shift, 2χ, is diluted by the increased volume of the modes. In Fig. 3c, we inject a coherent state into the highlighted mode in Fig. 3a and then perform qubit spectroscopy

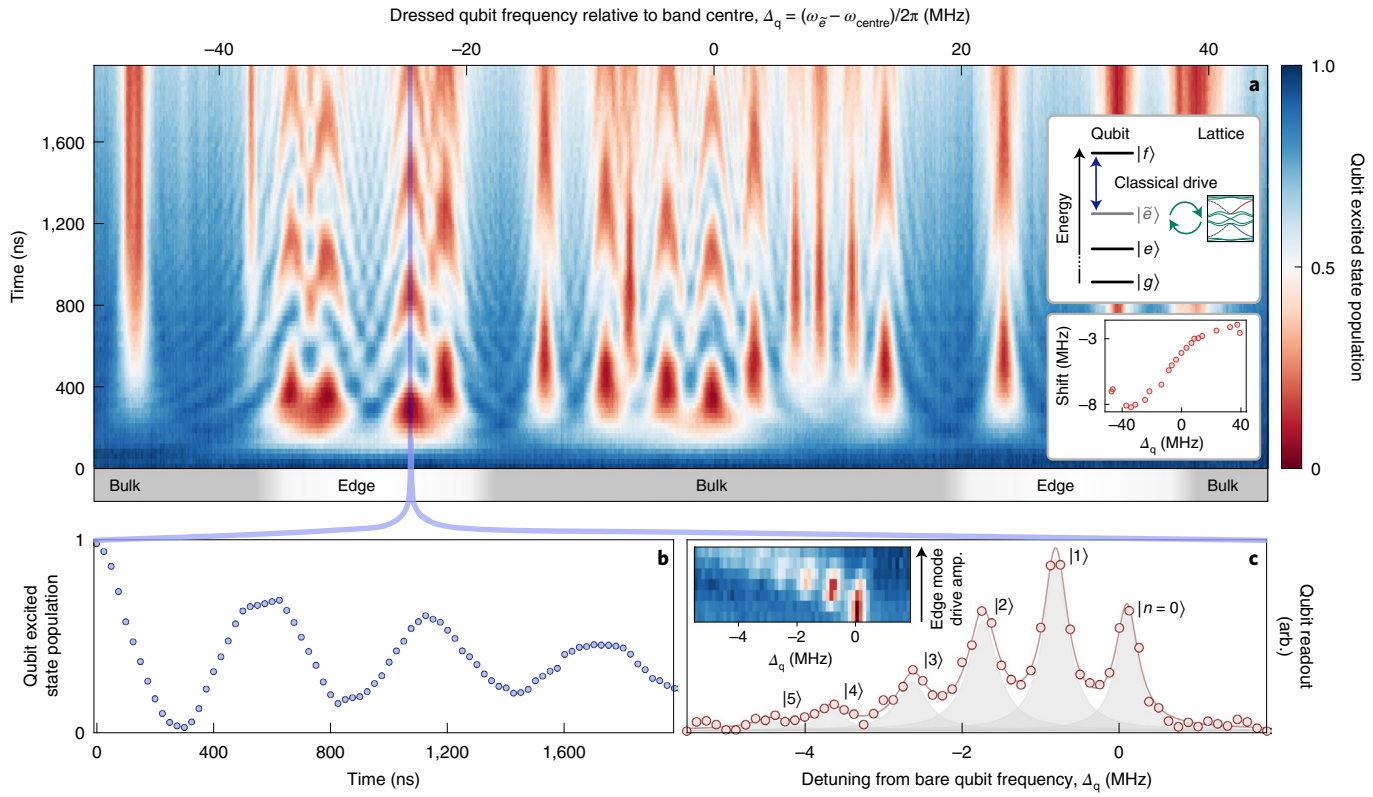

Fig. 3 | Quantum nonlinear dynamics on a chiral lattice. When a transmon qubit is coupled to the edge of the topological lattice, many of the properties of the (nonlinear) qubit are transferred to the (linear) lattice modes. **a**, The qubit is prepared in its second excited state $|f\rangle$ and driven with a classical tone (Methods), thereby scanning the energy of the resulting dressed excited state $|\tilde{e}\rangle$ through the band structure. A schematic of this process is provided in the top inset; the dressed excited state is positioned within the transmon energy level structure (at left) and on resonance with some mode of the lattice band structure (at right). The qubit can then coherently exchange a single photon with individual lattice modes. The resulting multimode chevron exhibits fast, low-amplitude Rabi oscillations when the qubit is detuned from the lattice modes and slower, high-contrast oscillations on resonance with each mode. The vacuum coupling to each mode is proportional to that mode's overlap with the qubit site (Supplementary Information K). As such, the edge modes exhibit fast oscillations while many bulk modes exhibit slower oscillations. The bottom inset shows the Lamb shift of the transmon due to the topological lattice vacuum, measured as the frequency differences between chevrons and linear spectroscopy in Fig. 2. The chevrons exhibit an additional overall Stark shift from the classical drive. The grey and white bar at the bottom highlights band and gap locations. **b**, When the qubit $|\tilde{e}\rangle$ state approaches resonance with a lattice mode (**a**, blue line), vacuum-stimulated Rabi oscillations between qubit and cavity arise, demonstrating strong-coupling cavity QED where information exchange with a single chiral mode is faster than all decay processes. **c**, To count photons in an edge mode (here the highlighted mode in **a**), we excite that mode directly with a coherent pulse and detect the number of photons it contains as a discrete photon-number-dependent shift of the qubit frequency (probed through its readout cavity, see Supplementary Information G). The multi-Lorentzian fit and individual Lorentzians for each photon number are shown in grey. Inset: by measuring the qubit excitation spectrum versus the drive amplitude applied to this edge mode, we observe a transition from vacuum (single, high-frequency resonance) to the expected Poisson distribution (multiple, lower-frequency resonances). Uncertainties are smaller than data points in **b** and **c** (Supplementary Information M).

to count the number of photons within the mode. The observed spectrum corresponds to a coherent state with $\bar{n} \approx 1.4$, with the individual photon occupancies clearly resolved. Indeed, when we perform this experiment as a function of the amplitude of the coherent excitation pulse (Fig. 3c, inset), we find a continuous evolution from vacuum into a Poisson distribution over the first six Fock states.

Outlook

In this work, we have demonstrated a photonic materials platform that combines synthetic magnetic fields for lattice-trapped photons with a single emitter. This has enabled us to explore interactions between the individual modes of a topological system and the nonlinear excitation spectrum of the emitter, entering the realm of fully granular chiral cavity QED and thus demonstrating the ability to count and manipulate individual photons in each mode of the lattice. We anticipate that coupling a transmon to a longer edge would enable qubit-mediated photon-induced deformation of the edge channel (in the 'super-strong-coupling' limit of the edge channel[30,34]), as well as universal quantum computation via time-bin-encoding[35] or blockade engineering[36]. Introduction of a qubit into the bulk of this system would allow investigation of the shell structure of a Landau-photon polariton[11], a precursor to Laughlin states. Addition of a second qubit on the edge would allow chiral, backscattering-immune quantum communication between the qubits[33]. Scaling up to one qubit per site will enable dissipative stabilization[37–40] of fractional Chern states of light[10] and thereby provide a clean platform for creating anyons and probing their statistics[41].

Online content

Any methods, additional references, Nature Research reporting summaries, source data, extended data, supplementary information, acknowledgements, peer review information; details of

author contributions and competing interests; and statements of data and code availability are available at https://doi.org/10.1038/s41567-022-01671-3.

Received: 19 September 2021; Accepted: 10 June 2022;
Published online: 28 July 2022

References

1. Walther, H., Varcoe, B. T., Englert, B.-G. & Becker, T. Cavity quantum electrodynamics. *Rep. Prog. Phys.* **69**, 1325–1382 (2006).
2. Von Klitzing, K. The quantized Hall effect. *Rev. Mod. Phys.* **58**, 519–531 (1986).
3. Stormer, H. L., Tsui, D. C. & Gossard, A. C. The fractional quantum Hall effect. *Rev. Mod. Phys.* **71**, S298–S305 (1999).
4. Hasan, M. Z. & Kane, C. L. Colloquium: topological insulators. *Rev. Mod. Phys.* **82**, 3045–3067 (2010).
5. Hofstadter, D. R. Energy levels and wave functions of Bloch electrons in rational and irrational magnetic fields. *Phys. Rev. B* **14**, 2239–2249 (1976).
6. Reagor, M. et al. Rea ching 10 ms single photon lifetimes for superconducting aluminum cavities. *Appl. Phys. Lett.* **102**, 192604 (2013).
7. Owens, C. et al. Quarter-flux Hofstadter lattice in a qubit-compatible microwave cavity array. *Phys. Rev. A* **97**, 013818 (2018).
8. Schuster, D. et al. Resolving photon number states in a superconducting circuit. *Nature* **445**, 515–518 (2007).
9. Lodahl, P. et al. Chiral quantum optics. *Nature* **541**, 473–480 (2017).
10. Anderson, B. M., Ma, R., Owens, C., Schuster, D. I. & Simon, J. Engineering topological many-body materials in microwave cavity arrays. *Phys. Rev. X* **6**, 041043 (2016).
11. De Bernardis, D., Cian, Z.-P., Carusotto, I., Hafezi, M. & Rabl, P. Light–matter interactions in synthetic magnetic fields: Landau-photon polaritons. *Phys. Rev. Lett.* **126**, 103603 (2021).
12. Carusotto, I. & Ciuti, C. Quantum fluids of light. *Rev. Mod. Phys.* **85**, 299–366 (2013).
13. Shomroni, I. et al. All-optical routing of single photons by a one-atom switch controlled by a single photon. *Science* **345**, 903–906 (2014).
14. Baur, S., Tiarks, D., Rempe, G. & Dürr, S. Single-photon switch based on Rydberg blockade. *Phys. Rev. Lett.* **112**, 073901 (2014).
15. Ozawa, T. et al. Topological photonics. *Rev. Mod. Phys.* **91**, 015006 (2019).
16. Abrikosov, A. A. The magnetic properties of superconducting alloys. *J. Phys. Chem. Solids* **2**, 199–208 (1957).
17. Rechtsman, M. C. et al. Photonic Floquet topological insulators. *Nature* **496**, 196–200 (2013).
18. Hafezi, M., Mittal, S., Fan, J., Migdall, A. & M., T. J. Imaging topological edge states in silicon photonics. *Nat. Photonics* **7**, 1001–1005 (2013).
19. Schine, N., Ryou, A., Gromov, A., Sommer, A. & Simon, J. Synthetic Landau levels for photons. *Nature* **534**, 671–675 (2016).
20. Schine, N., Chalupnik, M., Can, T., Gromov, A. & Simon, J. Electromagnetic and gravitational responses of photonic Landau levels. *Nature* **565**, 173–179 (2019).
21. Jia, N., Owens, C., Sommer, A., Schuster, D. & Simon, J. Time- and site-resolved dynamics in a topological circuit. *Phys. Rev. X* **5**, 021031 (2015).
22. Lu, Y. et al. Probing the Berry curvature and Fermi arcs of a Weyl circuit. *Phys. Rev. B* **99**, 020302 (2019).
23. Wang, Z., Chong, Y., Joannopoulos, J. D. & Soljacic, M. Observation of unidirectional backscattering-immune topological electromagnetic states. *Nature* **461**, 772–775 (2009).
24. Roushan, P. et al. Chiral ground-state currents of interacting photons in a synthetic magnetic field. *Nat. Phys.* **13**, 146–151 (2016).
25. Carusotto, I. et al. Photonic materials in circuit quantum electrodynamics. *Nat. Phys.* **16**, 268–279 (2020).
26. Clark, L. W., Schine, N., Baum, C., Jia, N. & Simon, J. Observation of Laughlin states made of light. *Nature* **582**, 41–45 (2020).
27. Ma, R. et al. A dissipatively stabilized Mott insulator of photons. *Nature* **566**, 51–57 (2019).
28. Barik, S. et al. A topological quantum optics interface. *Science* **359**, 666–668 (2018).
29. Barik, S., Karasahin, A., Mittal, S., Waks, E. & Hafezi, M. Chiral quantum optics using a topological resonator. *Phys. Rev. B* **101**, 205303 (2020).
30. Meiser, D. & Meystre, P. Superstrong coupling regime of cavity quantum electrodynamics. *Phys. Rev. A* **74**, 065801 (2006).
31. Kuzmin, R., Mehta, N., Grabon, N., Mencia, R. & Manucharyan, V. E. Superstrong coupling in circuit quantum electrodynamics. *npj Quantum Inf.* **5**, 1–6 (2019).
32. Fragner, A. et al. Resolving vacuum fluctuations in an electrical circuit by measuring the Lamb shift. *Science* **322**, 1357–1360 (2008).
33. Lamb Jr, W. E. & Retherford, R. C. Fine structure of the hydrogen atom by a microwave method. *Phys. Rev.* **72**, 241–243 (1947).
34. Sundaresan, N. M. et al. Beyond strong coupling in a multimode cavity. *Phys. Rev. X* **5**, 021035 (2015).
35. Pichler, H., Choi, S., Zoller, P. & Lukin, M. D. Universal photonic quantum computation via time-delayed feedback. *Proc. Natl Acad. Sci. USA* **114**, 11362–11367 (2017).
36. Chakram, S. et al. Multimode photon blockade. *Nat. Phys.* (2022). https://doi.org/10.1038/s41567-022-01630-y
37. Ma, R., Owens, C., Houck, A., Schuster, D. I. & Simon, J. Autonomous stabilizer for incompressible photon fluids and solids. *Phys. Rev. A* **95**, 043811 (2017).
38. Kapit, E., Hafezi, M. & Simon, S. H. Induced self-stabilization in fractional quantum Hall states of light. *Phys. Rev. X* **4**, 031039 (2014).
39. Hafezi, M., Adhikari, P. & Taylor, J. M. Chemical potential for light by parametric coupling. *Phys. Rev. B* **92**, 174305 (2015).
40. Lebreuilly, J. et al. Stabilizing strongly correlated photon fluids with non-Markovian reservoirs. *Phys. Rev. A* **96**, 033828 (2017).
41. Wilczek, F. *Fractional Statistics and Anyon Superconductivity* (World Scientific, 1990).

Methods

To achieve the highest quality factors, the structure for the chiral lattice is machined from a single block of high-purity (residual resistivity ratio 300) niobium. It is cooled to 30 mK (below the Nb superconducting transition at 9.2 K) to reduce loss and eliminate blackbody photons (Supplementary Information A). Sites are realized as coaxial resonators, while tunnelling between adjacent sites is achieved via hole coupling through the back side. As in ref. [41], the coupling holes are sub-wavelength and thus do not lead to leakage out of the structure. *s* orbital sites are implemented as single post resonators, while $p_x + ip_y$ sites are realized with three posts in the same resonator, coupled to a yttrium iron garnet (YIG) ferrimagnet that energetically isolates the $p_x + ip_y$ mode from the (vestigial) $p_x - ip_y$ and *s* modes (Fig. 1b and Supplementary Fig. S3). The T-symmetry of the ferrimagnet is broken with the ~0.2 T magnetic field of ∅1.6 mm N52 rare-earth magnets placed outside of the cavity, as close to the YIG as possible to minimize quenching of superconductivity[42,43] (Supplementary Fig. S4).

The transmon qubit (Supplementary Information B) has a $|g\rangle \leftrightarrow |e\rangle$ transition frequency of $\omega_q = 2\pi \times 7.8$ GHz, compared with the lattice spectrum centred on 8.9 GHz and spanning ±50 MHz (due to lattice tunnelling $J = 2\pi \times 18$ MHz). In the presence of the applied magnetic fields, the $|g\rangle \leftrightarrow |e\rangle$ transition of the transmon exhibits a T_1 value of 2.9 µs and T_2 value of 3.9 µs (Supplementary Information G). The anharmonicity of the transmon is $\alpha_q = 2\pi \times 346$ MHz. The transmon is coupled to its readout cavity ($\omega_r = 2\pi \times 10.6$ GHz, $\kappa_r = 2\pi \times 500$ kHz) with $g_r = 2\pi \times 66$ MHz. The transmon is coupled to the (1, 1) site of the lattice with $g_l = 2\pi \times 111$ MHz. The *s*-like lattice sites have a linewidth of $\kappa_s = 2\pi \times 5$ kHz, while the $p_x + ip_y$-like sites have a linewidth of $\kappa_{p_x+ip_y} = 2\pi \times 50$ kHz. The lattice sites themselves are tuned with ±1 MHz accuracy for the *s* sites and ±3 MHz accuracy for the $p_x + ip_y$ sites.

We perform linear spectroscopy of the lattice with dipole antennas inserted into each lattice site and use cryogenic switches to choose which sites we excite/probe (Supplementary Information C and F).

We perform nonlinear spectroscopy by exciting the transmon through its readout cavity. The transmon is fixed-frequency to avoid unnecessary dephasing from sensitivity to the magnetic fields applied to the YIG spheres. As a consequence, we 'tune' the transmon to various lattice modes by dressing through the readout cavity[25]. We prepare the transmon in the second excited ($|f\rangle$) state and then provide a detuned drive on the $|f\rangle \leftrightarrow |e\rangle$ transition to create a dressed $|\tilde{e}\rangle \approx |f\rangle - \frac{\Omega}{\Delta}|e\rangle$ state at any energy in the vicinity of the lattice band structure, with a dipole moment for coupling to the lattice which is rescaled by the ratio of the dressing Rabi frequency to the detuning from the $|f\rangle \leftrightarrow |e\rangle$ transition. The resulting vacuum-stimulated $|f, 0\rangle \leftrightarrow |g, 1_k\rangle$ Rabi frequency $g_k \approx \sqrt{2}\frac{g_l \alpha_q}{\Delta(\Delta+\alpha_q)}\Omega \times \langle x_{transmon}|\psi_k\rangle$. Here, Ω is the Rabi frequency of the dressing tone on the $|f\rangle \leftrightarrow |e\rangle$ transition of the transmon and $\langle x_{transmon}|\psi_k\rangle$ is the participation within mode k of the lattice site where the transmon resides. The dressing scheme may alternatively be understood as a two-photon Rabi process, where the $|f, 0\rangle \leftarrow |e, 0\rangle$ transition is stimulated by the classical drive and the $|e, 0\rangle \leftarrow |g, 1_k\rangle$ transition is stimulated by the vacuum field of mode *k*.

For the qubit measurements, the lattice is tuned to a centre frequency of $2\pi \times 8.9$ GHz, corresponding to a dressing frequency of $2\pi \times 6.35$ GHz ± 50 MHz. Note that, with the additional significant figure, the $|g\rangle \leftrightarrow |e\rangle$ transition has a frequency of $2\pi \times 7.75$ GHz.

Data availability

The experimental data presented in this manuscript are available from the corresponding author upon request, due to the proprietary file formats employed in the data collection process.

Code availability

The source code for simulations in Fig. 2 is available from the corresponding author upon request.

References

42. Chakram, S. et al. Seamless high-*Q* microwave cavities for multimode circuit quantum electrodynamics. *Phys. Rev. Lett.* **127**, 107701 (2021).
43. Pechal, M. et al. Microwave-controlled generation of shaped single photons in circuit quantum electrodynamics. *Phys. Rev. X* **4**, 041010 (2014).

Acknowledgements

This work was supported primarily by ARO MURI W911NF-15-1-0397 and AFOSR MURI FA9550-19-1-0399. This work was also supported by NSF EAGER 1926604, and the University of Chicago Materials Research Science and Engineering Center, which is funded by National Science Foundation under award no. DMR-1420709. J.C.O., M.G.P. and G.R. acknowledge support from the NSF GRFP. We acknowledge A. Oriani for providing a rapidly cycling refrigerator for cryogenic lattice calibration.

Author contributions

The experiments were designed by R.M., J.C.O., D.I.S. and J.S. The apparatus was built by J.C.O., R.M., G.R. and B.S. J.C.O. and M.G.P. collected the data, and all authors analysed the data and contributed to the manuscript.

Competing interests

The authors declare no competing financial interests.

Additional information

Supplementary information The online version contains supplementary material available at https://doi.org/10.1038/s41567-022-01671-3.

Correspondence and requests for materials should be addressed to David I. Schuster.

Peer review information *Nature Physics* thanks Sunil Mittal and Yutaka Tabuchi for their contribution to the peer review of this work.

Reprints and permissions information is available at www.nature.com/reprints.